

Fractal and complex network analyses of protein molecular dynamics

Yuan-Wu Zhou^{1,2}, Jin-Long Liu¹, Zu-Guo Yu^{1,3*}, Zhi-Qin Zhao¹ and Vo Anh³

¹Hunan Key Laboratory for Computation and Simulation in Science and Engineering and Key Laboratory of Intelligent Computing and Information Processing of Ministry of Education, Xiangtan University, Xiangtan, Hunan 411105, China.

²Civil Construction Engineering Department, Guangxi University of Science and Technology, Liuzhou 545000, China.

³School of Mathematical Sciences, Queensland University of Technology, GPO Box 2434, Brisbane, Q4001, Australia.

Abstract

Based on protein molecular dynamics, we investigate the fractal properties of energy, pressure and volume time series using the multifractal detrended fluctuations analysis (MF-DFA) and the topological and fractal properties of their converted horizontal visibility graphs (HVGs). The energy parameters of protein dynamics we considered are bonded potential, angle potential, dihedral potential, improper potential, kinetic energy, Van der Waals potential, electrostatic potential, total energy and potential energy. The shape of the $h(q)$ curves from MF-DFA indicates that these time series are multifractal. The numerical values of the exponent $h(2)$ of MF-DFA show that the series of total energy and potential energy are non-stationary and anti-persistent; the other time series are stationary and persistent apart from series of pressure (with $H \approx 0.5$ indicating the absence of long-range correlation). The degree distribution of their converted HVGs show that these networks are exponential. The results of fractal analysis show that fractality exists in these converted HVGs. For each energy, pressure or volume parameter, it is found that the values of $h(2)$ of MF-DFA on the time series, exponent λ of the exponential degree distribution and fractal dimension d_B of their converted HVGs do not change much for different proteins (indicating some universality). We also found that after taking average over all proteins, there is a linear relationship between $\langle h(2) \rangle$ (from MF-DFA on time series) and $\langle d_B \rangle$ of the converted HVGs for different energy, pressure and volume.

Key words: protein molecular dynamics; multifractal detrended fluctuation analysis; horizontal visibility graph; fractal analysis; degree distribution.

1 Introduction

Proteins are among the most important biomacromolecules because they can perform biological functions, which are usually determined by their structures. To date, structures of 97362 proteins (updated in Protein Data Bank [1] on 2014-01-28) have been obtained by experimental methods,

*Corresponding to yuzuguo@aliyun.com

such as X-ray (88.4%), solution NMR (10.6%) and electron microscopy (0.7%). On the other hand, molecular dynamics simulation packages such as NAMD (*Not (just) Another Molecular Dynamics program*) [2] has been developed to learn about different aspects of proteins. Protein molecule energy includes kinetic energy and potential energy, and potential energy can be calculated by quasi-empirical way (such as CHARMM [3] and AMBER [4]). In fact, Rueda *et al.* [5] used NAMD to analyze the molecular dynamics of 30 real proteins. This paper uses NAMD to simulate protein molecular dynamics, then derive the time series for some corresponding parameters whose features reflect the aspects of protein structures.

Apart from being characterized by an enormous number of degrees of freedom, proteins have multidimensional potential energy surfaces [6]. It is well known that the self-similarity exhibiting in the distributions of their biophysical and biochemical properties can serve as an effective tool to extract the inherently inhomogeneous and nonlinear behaviors of protein structures. Fractal dimension (FD) has been widely used to characterize the self-similarity of fractal objects [7, 8]. Many FD-based methods have been proposed to investigate protein structures [6]. Fractal methods can also be used to characterize the scaling properties of time series and then to reveal the self-similarity of the original system [7]. A multifractal system is a generalization of a fractal system in which a single exponent (the fractal dimension) is not enough to describe its dynamics; instead, a continuous spectrum of exponents (the so-called singularity spectrum) is needed [9]. The concept of multifractal phenomena describes that different regions of an object have different fractal properties, and multifractal scaling provides a quantitative description of a broad range of heterogeneous phenomena [10]. Multifractal analysis was initially proposed to treat turbulence data and is a useful way to characterize the spatial heterogeneity of both theoretical and experimental fractal patterns [11]. The multifractal detrended fluctuations analysis (MF-DFA) [12] is an extension of the standard detrended fluctuation analysis (DFA) introduced by Peng *et al.* [13, 14]. DFA can be employed to detect long-range correlations in stationary and nonstationary time series. Hence MF-DFA is a suitable tool to characterize the multifractal property and long-range correlation in time series. Multifractal analysis has been used to study genomes [15-17], protein structures and functions (e.g. [18-22]). In this paper, we investigate by MF-DFA [12] the scaling property of the associated time series of energy, pressure and volume derived from simulations of protein molecular dynamics.

In last decade, the study of complex networks has gained prominence across many disciplines of science. Studies have shown that complex network theory has become a powerful tool to analyze protein complex structures [23-25]. Single proteins in 3D space can also be considered as biological complex systems emerged through the interactions of their constituent amino acids. These interactions among the amino acids within a protein can be presented as residues interaction network (RIN) (also called residues interaction graphs (RIGs), protein contact network (PCN), protein structure network (PSN), protein contact map (PCM), amino acid network (AAN)), which can be constructed with varying definitions of nodes and edges [23-25].

Recent studies showed that complex network theory (such as recurrence networks) may also be an effective method to analyze time series [26-33]. Lacasa *et al.* [26] proposed the visibility graph (VG) algorithm to convert time series into complex networks. Then Luque *et al.* [27] proposed the horizontal visibility algorithm to convert time series into complex networks. It has been shown that these converted networks inherit several properties of time series in the structure of networks [34-36]. Therefore, we can understand time series from a new point of view using the converted networks. In

this paper, we hope to reveal some meaningful information in the associated time series of energy, pressure and volume for real proteins from the perspective of the horizontal visibility graphs (HVGs) [27]. This prompts us to further study the fundamental topological and fractal properties of the converted HVGs from different energy, pressure and volume time series of real proteins.

The fractal and self-similarity properties of complex network have also been focused and studied widely in a variety of fields [37-39]. It is found that many complex networks, including the world-wide web (WWW), social networks, protein-protein interaction (PPI) networks and cellular networks, are self-similar under a certain length-scale. Some numerical algorithms have been proposed to calculate the fractal dimensions of complex networks. Song *et al.* [40] proposed a box-counting algorithm to calculate their fractal dimension. Kim *et al.* [41] studied the skeleton and fractal scaling in complex networks via an improvement method. Later on, Zhou *et al.* [42] introduced an alternative algorithm to detect self-similarity of cellular networks. Recently, Li *et al.* [43] studied the fractal properties of a family of fractal networks using the random sequential box-covering algorithm proposed by Kim *et al.* [41]. Liu *et al.* [33] adopted this algorithm to calculate the fractal dimensions of the recurrence networks constructed from fractional Brownian motions. In this paper, we also adopting the random sequential box-covering algorithm to calculate the fractal dimension of the converted HVGs of the time series of energy, pressure and volume for real proteins.

2 Molecular dynamics for protein

The behavior of biomolecular systems can be modelled by molecular dynamics, which is helpful to understand protein functions. A common procedure of molecular dynamics [44] for proteins is as follows:

(a) Initialize the positions and velocities of all atoms. The initial positions of atoms come from Protein Data Bank (PDB [1]). Add water and ions to a box with protein, minimize the box system energy. Then, the initial velocities of atoms are assigned from Maxwell’s distribution.

(b) Calculate forces for all atoms using potential energy. The protein potential energy can be defined as

$$V = V_{bonds} + V_{angles} + V_{dihedrals} + V_{impropers} + V_{Vdw} + V_{electrostatic}, \quad (1)$$

where V is protein potential energy, V_{bonds} is bonded potential, V_{angles} is angle potential, $V_{dihedrals}$ is dihedral potential, $V_{impropers}$ is improper potential, V_{Vdw} is Van der Waals potential, and $V_{electrostatic}$ is electrostatic potential. In this paper, we analyze the potential energy and kinetic energy time series. Then, forces that act on an atom can be written as

$$\vec{F} = \frac{\partial V(\vec{r})}{\partial \vec{r}}, \quad (2)$$

where \vec{r} is the position vector of atoms.

(c) Apply thermostat and volume changes. Update positions and velocities. According to Newton’s law, the kinetic equation can be written as

$$\vec{F} = m \frac{\partial^2 \vec{r}}{\partial t^2}. \quad (3)$$

Using an algorithm, such as the Verlet algorithm or LeapFrog algorithm, new positions and velocities can be calculated.

(d) Repeat steps (b) and (c) till a termination condition is met.

(e). Analyze data. NAMD is a software for biomolecular molecular dynamics [2]. Some researchers used NAMD to achieve some important results [5]. In the paper, we use it to simulate protein dynamics.

3 Multifractal detrended fluctuation analysis for time series

Detrended fluctuations analysis (DFA) introduced by Peng *et al.* [13, 14] can be employed to detect long-range correlations in stationary and nonstationary time series. The multifractal detrended fluctuations analysis (MF-DFA) [12] is an extension of DFA. This approach can be described as follows. Given a time series x_k , $k = 1, \dots, N$, where N is the length of the series, the profile $Y(i)$ is defined as

$$Y(i) \equiv \sum_{k=1}^i [x_k - \langle x \rangle]. \quad i = 1, \dots, N, \quad (4)$$

where $\langle x \rangle$ is the mean of sequence x_k . Then $Y(i)$ is divided into $N_s \equiv \text{int}(N/s)$ non-overlapping and continuous segments of equal length s . Then we estimate the variance of $y(i)$ by

$$F^2(s, v) \equiv \frac{1}{s} \sum_{i=1}^s \{Y[(v-1)s + i] - y_v(i)\}^2, \quad (5)$$

for each segment v , $v = 1, \dots, N$ and

$$F^2(s, v) \equiv \frac{1}{s} \sum_{i=1}^s \{Y[N - (v - N_s)s + i] - y_v(i)\}^2, \quad (6)$$

for $v = N_s + 1, \dots, 2N_s$, where $y_v(i)$ is a fitting polynomial in segment v (linear, quadratic, cubic, or higher order polynomial). Last we take the average over $2N_s$ segments to achieve the q th order fluctuation function

$$F_q(s) \equiv \left\{ \frac{1}{2N_s} \sum_{v=1}^{2N_s} [F^2(s, v)]^{q/2} \right\}^{1/q}, \quad (\text{if } q \neq 0). \quad (7)$$

$$F_q(s) \equiv \exp\left\{ \frac{1}{4N_s} \sum_{v=1}^{2N_s} \ln[F^2(s, v)] \right\}, \quad (\text{if } q = 0). \quad (8)$$

We will assume that $F_q(s)$ is characterized by a power law:

$$F_q(s) \propto s^{h(q)}. \quad (9)$$

The scaling function $h(q)$ is then determined by the regression of $\ln F_q(s)$ on $\ln s$ in some range of time scale s .

MF-DFA is suitable for both stationary and nonstationary time series [12]. We denote by H the Hurst exponent of time series. The range $0.5 < H < 1$ indicates persistence; and the range $0 < H < 0.5$ indicates anti-persistence; for uncorrelated series, the scaling exponent H is equal

to 0.5 [45]. Assuming the setting of fractional Brownian motion, Movahed *et al.* [46] proved the relation $H = h(2) - 1$ between H and the exponent $h(2)$ for small scales. In the case of fractional Gaussian noise, it was shown that $H = h(2)$ [46]. Hence we can use the value of H calculated from $h(2)$ to detect the nature of long-range correlation (LRC) in time series under the assumption of fractional Gaussian noise or fractional Brownian motion.

4 Complex networks: horizontal visibility graph for time series

A graph (or network) is a collection of nodes, which denote the elements of a system, and links or edges, which identify the relations or interactions among these elements.

Inspired by the concept of visibility [47], Lacasa *et al.* [26] proposed a simple computational method to convert a time series into a network, known as visibility graph (VG). It has been shown that time series structures are inherited in the associated graphs, such as periodic, random, and fractal series map into regular, random, and scale-free networks respectively [26]. In addition, the degree distributions of the VGs constructed from random series by a uniform distribution in $[0, 1]$ have exponential tails $P(k) \sim \exp(-\lambda k)$ [26]. For this case, the greater the value of λ is, the faster attenuation of $P(k)$ is along with k . In contrast, the degree distributions of the VGs converted from fractional Brownian motions have power-law tails $P(k) \sim k^{-\alpha}$ [34].

Then a simplification of VG algorithm was proposed to map a time series into a horizontal visibility graph (HVG) [27]. A HVG is obtained from the mapping of a time series into a network according to the following horizontal visibility criterion: Given a time series $\{x_1, x_2, \dots, x_N\}$, two arbitrary data points x_i and x_j in the time series have horizontal visibility, and consequently become two connected nodes in the associated graph, if any other data point x_n such that $i < n < j$ fulfils

$$x_i, x_j > x_n. \quad (10)$$

Thus a connected, unweighted network can be constructed from a time series and is called its *horizontal visibility graph* (HVG). In fact, the HVG of a given time series is always a subgraph of its associated VG. Luque *et al.* [27] have shown that the degree distribution of a HVG constructed from any random series has an exponential form $P(k) = (3/4)\exp(-k \ln(3/2))$. Then Lacasa *et al.* [35] used the horizontal visibility algorithm to characterize and distinguish between correlated, uncorrelated and chaotic processes. They showed that in every case the series maps into a graph with exponential degree distribution $P(k) \sim \exp(-\lambda k)$, where the value of λ characterizes the specific process [35]. In this paper, we adopt the horizontal visibility algorithm to convert the time series of energy, pressure and volume into HVGs.

5 Fractal analysis of horizontal visibility graph (complex networks)

The random sequential box-covering algorithm proposed by Kim *et al.* [41] is an efficient algorithm for fractal analysis of complex networks. Recently, our group used this algorithm to study the fractal properties of a family of fractal networks and recurrence networks constructed from fractional Brownian motions [33, 43].

For a given HVG or network, we let $N_B(r)$ be the minimum number of boxes with size r which are needed to cover the entire network. If the power-law relation $N_B(r) \sim r^{-d_B}$ holds for some

scaling-range of r and constant d_B , we say that the fractality exists in this network, and d_B is called its fractal dimension. So, in practice, we often obtain the fractal dimension d_B by fitting the linear relationship between $N_B(r)$ and r in a log-log plot.

Before using the random sequential box-covering algorithm to calculate the fractal dimension of a network, we need to use Floyd’s algorithm [48] or Dijkstra’s algorithm of MatLab toolbox to calculate the shortest-path distance matrix D of this network according to its adjacency matrix A . The random sequential box-covering algorithm [41] can be summarized as follows.

(I) Ensure that all nodes in the network are not covered, and no node has been selected as the center of a box.

(II) Denote the size of the network as N . We set $t = 1, 2, \dots, T$; here we take $T = 1000$. Then we rearrange the nodes into $T = 1000$ different random orders. That is to ensure that the nodes of a network are randomly chosen as center nodes.

(III) Set the radius r of boxes which will be used to cover the nodes in the range $[1, d]$, where d is the diameter of the network (i.e. the longest distance between nodes in the network).

(IV) Treat the nodes of the t th kind of random orders that we have obtained in (II) as the center of a box successively, then search all the other nodes. If a node has a distance within r to the center node and has not been covered yet, then cover it.

(V) If no more new nodes can be covered by this box, then we abandon this box.

(VI) Repeat (IV) - (V) until all the nodes are covered by the corresponding boxes. We denote the number of boxes in this box covering as $N(t, r)$.

(VII) Repeat steps (III) and (VI) for all the random orders to find a box covering with minimal number of boxes $N(t, r)$. Then denote this minimal number of boxes as $N_B(r/d)$.

(VIII) For different r , repeat (III)-(VII). Then we use the linear regression of $-\ln(N_B(r/d))$ vs $\ln(r/d)$ to estimate the fractal dimension of the HVG or network.

6 Results and discussion

We use a list of 29 proteins (without ligands, RNA, or DNA, greater than 100 amino acids) as in [5] to simulate their dynamics (see Table 1) by NAMD.

Using NAMD with energy step size $200fs$, protein structures from PDB were used as starting points for 10-ns production trajectories, performed at constant pressure (1atm) and temperature (310K) using standard coupling schemes (the same in all cases). CHARMM force fields were used in production runs. Then, we obtained time series of bonded potential, angle potential, dihedral potential, improper potential, electrostatic potential, Van der Waals potential, kinetic energy, total energy, potential energy, pressure, and volume. For example, we plotted the 11 time series of protein 1A3H in Figures 1 to 3.

Then we performed MF-DFA on these time series. As an example, we show how to estimate the exponents $h(q)$ for the bonded potential time series of protein 1A3H in Figure 4. The numerical results showed that the best fit occurs in the range $s \in [3, 22]$. So we used this scaling-range to calculate the exponents $h(q)$. We plotted the $h(q)$ curves for the energy, pressure and volume time series of protein 1A3H in Figure 5 as examples. From the shape of the $h(q)$ curves of these time series for all proteins, we found that all time series considered here are multifractal. Therefore

these time series are complicated and cannot be characterized by a single fractal dimension. In fact, they depict heterogeneous phenomena and different regions of each time series have different fractal properties [10]. In particular, the numerical values of $h(2)$ (which is related to the Hurst exponent H) are given in Table 2. The average values and standard deviations of $h(2)$ for all 11 parameters of 29 proteins are also listed in the bottom two rows of Table 2.

For energy parameters, the energy values are in *kcal/mol*, bonded potential $\sim 10^3$, angle potential $\sim 10^3$, dihedral potential $\sim 10^3$, improper potential $\sim 10^2$, electrostatic potential $\sim 10^5$, Van der Waals potential $\sim 10^4$, kinetic energy $\sim 10^4$, total energy $\sim 10^5$, and potential energy $\sim 10^5$. From Table 2, we can see that the series of total energy and potential energy are non-stationary ($h(2) > 1.0$) and anti-persistent ($0 < H = h(2) - 1 < 0.5$). The other time series are stationary and persistent apart from that of pressure (with $H \approx 0.5$ indicating the absence of long-range correlation). Among bonded potential, angle potential, dihedral potential, and improper potential, we can see that the LRC in the series of angle potential is the strongest and that in those of improper potential is the weakest, and the LRC in those of dihedral potential is stronger than that in those of bonded potential. Among the three largest energy parameters, namely the electrostatic potential, Vdw potential and kinetic energy, we find that the LRC in the series of electrostatic potential is the strongest and that in the series of Vdw potential is the weakest.

Remark 1: The NMR structures of many proteins in PDB were obtained from different models. For example, the structures of Protein 1WUZ in PDB were obtained from 30 NMR models. In this case, we always use the structure obtained from the 1st NMR model in the present study. We also tested the effect of different NMR models on our results. We simulated the 1st model, 10th model, 20th model, and 30th model of protein 1WUZ. Our numerical results of MF-DFA showed that the $h(q)$ curves for the four models are very close. And it should be required in PDB that the structures of any protein obtained from different NMR models should be similar to each other. Therefore, it is unlikely that different NMR models of proteins would affect our results.

Then, these time series were converted into HVGs. We denote k the degree of nodes, $P(k)$ the probability of degree k . We obtained the plots for the relations $k \sim P(k)$, $\ln(k) \sim \ln(P(k))$, and $k \sim \ln(P(k))$, and found that only the linear relationship in the $k \sim \ln(P(k))$ plots is reasonable. We gave the degree distributions $P(k)$ of the HVGs for the angle potential and pressure time series of protein 1A3H in Figure 6 as examples. So the HVGs of these parameters are exponential networks. We gave the numerical values of the exponent λ in Table 3. The average values and standard deviations of λ for all 11 parameters of the 29 proteins are also given in Table 3. Among the three largest energy parameters, namely the electrostatic potential, Vdw potential and kinetic energy, the attenuation of the degree distribution for HVGs of electrostatic potential is the fastest. The degree distribution for HVGs of total energy has the fastest attenuation among all energy parameters. The degree distribution for HVGs of potential energy has the faster attenuation comparing to its components.

We also studied the fractal properties of the converted HVGs using the random sequential box-covering algorithm described in Section 5. We found that there is a scaling-range of r in which the power-law relation $N_B(r) \sim r^{-d_B}$ holds for all converted HVGs, hence the fractality exists in these networks. We showed how to estimate the fractal dimension d_B of HVGs constructed from the electrostatic potential and van der Waals potential time series of protein 1A3H in Figure 7 as examples. The fractal dimension d_B is the slope of linear regression between $-\ln(N_B(r/d))$ and

$\ln(r/d)$ for each case. In Table 4, we gave the fractal dimensions d_B for all time series we considered here. The bottom two rows of Table 4 are the average values and standard deviations of d_B for all 11 parameters of 29 proteins, respectively.

From Tables 2, 3 and 4, for each energy or pressure or volume parameter, one can find that the values of $h(2)$ of MF-DFA on the time series, exponent λ of exponential degree distribution and fractal dimension d_B of their converted HVGs do not change much for different proteins (indicating some universality). So these methods in this paper cannot be used for the prediction of protein structures and functions.

For 29 time series (29 proteins) of each kind of energy or pressure or volume, we calculated the average values of $h(2)$ (from MF-DFA on time series) and d_B the converted HVGs. Hence we obtained 11 values of $\langle h(2) \rangle$ and 11 values of $\langle d_B \rangle$ respectively. It is surprising that there is a nice linear relationship between $\langle h(2) \rangle$ and $\langle d_B \rangle$ as shown in Figure 8. The relationship can be well fitted by the linear formula:

$$\langle d_B \rangle = -1.5210 \times \langle h(2) \rangle + 3.1176.$$

7 Conclusions

Using the NAMD software, we derived the time series of bonded potential, angle potential, dihedral potential, improper potential, electrostatic potential, Van der Waals potential, kinetic energy, total energy, potential energy, pressure, and volume for each protein. The shape of the $h(q)$ curves from MF-DFA indicates that these time series are multifractal.

In particular, the numerical values of $h(2)$ of MF-DFA (which is related to the Hurst exponent H) show that the series of total energy and potential energy are non-stationary and anti-persistent; the other time series are stationary and persistent apart from the series of pressure (with $H \approx 0.5$ indicating the absence of long-range correlation).

The degree distributions of their converted HVGs show that these networks are exponential. Among the three largest energy parameters, namely the electrostatic potential, Vdw potential and kinetic energy, the attenuation of the degree distribution of electrostatic potential is the fastest. The degree distribution for HVGs of total energy has the fastest attenuation among all energy parameters. The degree distribution for HVGs of potential energy has the faster attenuation comparing to its components.

We found that there is a scaling-range of r in which the power-law relation $N_B(r) \sim r^{-d_B}$ holds for all converted HVGs, hence fractality exists in these networks.

For each energy, pressure or volume parameter, it is found that the values of $h(2)$ of MF-DFA on the time series, exponent λ of exponential degree distribution and fractal dimension d_B of their converted HVGs do not change much for different proteins (indicating some universality). So these methods cannot be used for the prediction of protein structures and functions.

After taking average over all proteins, we surprisingly found that there is a linear relationship between $\langle h(2) \rangle$ (from MF-DFA on time series) and $\langle d_B \rangle$ of converted HVGs for different energy, pressure and volume.

ACKNOWLEDGEMENTS

This project was supported by the Natural Science Foundation of China (Grant No. 11371016); the Chinese Program for Changjiang Scholars and Innovative Research Team in University (PCSIRT) (Grant No. IRT1179); the Research Foundation of Education Commission of Hunan Province of China (Grant No. 11A122); the Lotus Scholars Program of Hunan province of China; postdoctoral research fund of Xiangtan University of China.

References

- [1] H.M. Berman, J. Westbrook, Z. Feng, G. Gilliland, T.N. Bhat, H. Weissig, I.N. Shindyalov, and P.E. Bourne, The protein data bank, *Nucleic acids research*, 28(1) (2000) 235-242.
- [2] J.C. Phillips, R. Braun, W. Wang, J. Gumbart, E. Tajkhorshid, E. Villa, C. Chipot, R.D. Skeel, L. Kale, and K. Schulten, Scalable molecular dynamics with NAMM, *J. Comput. Chem.*, 26(16) (2005) 1781-1802.
- [3] B.R. Brooks, C.L. Brooks, A.D. MacKerell Jr., *et al.*, CHARMM: the biomolecular simulation program, *J. Comput. Chem.*, 30(10) (2009) 1545-1614.
- [4] D.A. Case, T.E. Cheatham, T. Darden, H. Gohlke, R. Luo, K.M. Merz Jr., A. Onufriev, C. Simmerling, B. Wang, and R.J. Woods, The Amber biomolecular simulation programs, *J. Comput. Chem.*, 26(16) (2005) 1668-88.
- [5] M. Rueda, C. Ferrer-Costa, T. Meyer, A. Perez, J. Camps, A. Hospital, J.L. Gelpi, and M. Orozco, A consensus view of protein dynamics, *Proc. Natl. Acad. Sci. U.S.A.*, 104(3) (2007) 796-801.
- [6] A. Banerji and I. Ghosh, Fractal symmetry of protein interior: What have we learned? *Cell. Mol. Life Sci.*, 68 (2011) 2711-2737.
- [7] B.B. Mandelbrot, *The Fractal Geometry of Nature*, New York: Academic Press, 1983.
- [8] K.J. Falconer, *Techniques in Fractal Geometry*, New York: Wiley, 1997.
- [9] D. Harte, *Multifractals*, London: Chapman & Hall, 2001.
- [10] H.E. Stanley, P. Meakin, Multifractal phenomena in physics and chemistry (Review), *Nature*, 335: 405-409.
- [11] T.C. Halsey, M.H. Jensen, L.P. Kadanoff, I. Procaccia, and B.I. Shraiman, Fractal measures and their singularities: the characterization of strange sets, *Phys. Rev. A*, 33 (1986) 1141-1151.
- [12] J.W. Kantelhardt, S.A. Zschiegner, E. Koscielny-Bunde, A. Bunde, S. Havlin, and H.E. Stanley, Multifractal detrended fluctuation analysis of nonstationary time series, *Physica A*, 316(1) (2002) 87-114.
- [13] C.K. Peng, S.V. Buldyrev, A.L. Goldberger, S. Havlin, F. Sciortino, M. Simons, and H.E. Stanley, Long-range correlations in nucleotide sequences. *Nature*, 356 (1992) 168-170.
- [14] C.K. Peng, S.V. Buldyrev, S. Havlin, M. Simons, H.E. Stanley and A.L. Goldberger, Mosaic organization of DNA nucleotides. *Phys. Rev. E*, 49 (1994) 1685-1689.
- [15] Z.G. Yu, V. Anh, and K.S. Lau, Measure representation and multifractal analysis of complete genome, *Phys. Rev. E*, 64 (2001) 031903 .
- [16] Z.G. Yu, V. Anh, and K.S. Lau, Multifractal and correlation analysis of protein sequences from complete genome, *Phys. Rev. E*, 68 (2003) 021913.
- [17] Z.G. Yu, V. Anh, and K.S. Lau, Chaos game representation, and multifractal and correlation analysis of protein sequences from complete genome based on detailed HP model, *J. Theor. Biol.*, 226 (2004) 341-348.
- [18] J.S. Balafas and T.G. Dewey, Multifractal analysis of solvent accessibilities in proteins, *Phys. Rev. E.*, 52 (1995) 880-887.
- [19] Z.G. Yu, V. Anh, K.S. Lau, and L.Q. Zhou, Fractal and multifractal analysis of hydrophobic free energies and solvent accessibilities in proteins, *Phys. Rev. E.*, 73 (2006) 031920.
- [20] J.Y. Yang, Z.G. Yu, and V. Anh, Clustering structure of large proteins using multifractal analyses based on 6-letters model and hydrophobicity scale of amino acids, *Chaos, Solitons and Fractals*, 40 (2009) 607-620.
- [21] J.Y. Yang, Z.L. Peng, Z.G. Yu, R.J. Zhang, V. Anh, and D. Wang, Prediction of protein structural classes by recurrence quantification analysis based on chaos game representation, *J. Theor. Biol.*, 257 (2009) 618-626.
- [22] S.M. Zhu, Z.G. Yu, and V. Anh, Protein structural classification and family identification by multifractal analysis and wavelet spectrum, *Chin. Phys. B*, 20 (2011) 010505.

- [23] G. Amitai, A. Shemesh, E. Sitbon, M. Shklar, D. Netanely, I. Venger, and S. Pietrokovski, Network analysis of protein structure identifies functional residue, *J. Mol. Biol.*, 344 (2004) 1135-1146.
- [24] A.R. Atilgan, P. Akan, and C. Baysal, Small-World communication of residues and significance for protein dynamics, *Biophys. J.*, 86 (2004) 85-91.
- [25] G. Bagler and S. Sinha, Network properties of protein structures, *Physica A*, 346 (2005) 27-33.
- [26] L. Lacasa, B. Luque, F. Ballesteros, J. Luque, and J.C. Nuño, From time series to complex networks: The visibility graph, *Proc. Natl. Acad. Sci. U.S.A.*, 105(13) (2008) 4972-4975.
- [27] B. Luque, L. Lacasa, F. Ballesteros, and J. Luque, Horizontal visibility graphs: Exact results for random time series, *Phys. Rev. E*, 80 (2009) 046103.
- [28] R.V. Donner, Y. Zou, J.F. Donges, N. Marwan, and J. Kurths, Recurrence networks: a novel paradigm for nonlinear time series analysis, *New J. Phys.*, 12 (2010) 033025.
- [29] R.V. Donner, Y. Zou, J.F. Donges, N. Marwan, and J. Kurths, Ambiguities in recurrence-based complex network representations of time series, *Phys. Rev. E*, 81 (2010) 015101(R).
- [30] R.V. Donner, J. Heitzig, J.F. Donges, Y. Zou, N. Marwan, and J. Kurths, The geometry of chaotic dynamics C a complex network perspective, *Eur. Phys. J. B*, 84 (2011) 653-672.
- [31] R.V. Donner, M. Small, J.F. Donges, N. Marwan, Y. Zou, R. Xiang and J. Kurths, Recurrence-based time series analysis by means of complex network methods, *Int. J. Bifurc. and Chaos*, 21(4) (2011) 1019-1046.
- [32] J.F. Donges, J.Heitzig, R.V. Donner, and J. Kurths, Analytical framework for recurrence network analysis of time series, *Phys. Rev. E*, 85 (2012) 046105.
- [33] J.L. Liu, Z.G. Yu and V. Anh, Topological properties and fractal analysis of recurrence network constructed from fractional Brownian motions, *Phys. Rev. E*, 89 (2014) 032814.
- [34] L. Lacasa, B. Luque, J. Luque, and J.C. Nuño, The visibility graph: a new method for estimating the Hurst exponent of fractional Brownian motion, *EPL(Europhys. Lett)*, 86 (2009) 30001.
- [35] L. Lacasa and R. Toral, Description of stochastic and chaotic series using visibility graphs, *Phys. Rev. E*, 82 (2010) 036120.
- [36] W.J. Xie and W.X. Zhou, Horizontal visibility graphs transformed from fractional Brownian motions: Topological properties versus the Hurst index, *Physica A*, 390 (2011) 3592-3601.
- [37] G. Palla, I. Derenyi, I. Farkas, and T. Vicsek, Uncovering the overlapping community structure of complex networks in nature and society, *Nature*, 435(7043) (2005) 814-818.
- [38] C. Song, S. Havlin and H.A. Makse, Self-similarity of complex networks, *Nature*, 433 (2005) 392-395.
- [39] K.I. Goh, G. Salvi, B. Kahng, and D. Kim, Skeleton and fractal scaling in complex networks, *Phys. Rev. Lett.*, 96(1) (2006) 018701.
- [40] C. Song, L.K. Gallos, S. Havlin and H.A. Makse, How to calculate the fractal dimension of a complex network: the box covering algorithm, *J. Stat. Mech.: Theor. Exp.*, 3 (2007) P03006.
- [41] J.S. Kim, K.I. Goh, G. Salvi, E. Oh, B. Kahng and D. Kim, Fractality in complex networks: Critical and supercritical skeletons, *Phys. Rev. E*, 75 (2007) 016110.
- [42] W.X. Zhou, Z.Q. Jiang, and D. Sornette, Exploring self-similarity of complex cellular networks: The edge-covering method with simulated annealing and log-periodic sampling, *Physica A*, 375(2) (2007) 741-752.
- [43] B.G. Li, Z.G. Yu and Y. Zhou, Fractal and multifractal properties of a family of fractal networks, *J. Stat. Mech.: Theor. Exp.*, 2014 (2014) P02020.
- [44] A. Kumar, Molecular Dynamics Simulations, [http://www.personal.psu.edu/auk183/MolDynamics/Molecular%20Dynamic s%20Simulations.html](http://www.personal.psu.edu/auk183/MolDynamics/Molecular%20Dynamic%20Simulations.html).
- [45] B.B. Mandelbrot and J.W. Van Ness, Fractional Brownian motions, fractional noises and applications, *SIAM Rev.*, 10(4) (1968) 422-437.
- [46] M.S. Movahed, G.R. Jafari, F. Ghasemi, S. Rahvar, and M.R.R. Tabar, Multifractal detrended fluctuation analysis of sunspot time series, *J. Stat. Mech.: Theory exper.* 2 (2006) P02003.
- [47] M. de Berg, M. van Kreveld, M. Overmans, and O. Schwarzkopf: *Computational Geometry: Algorithms and Applications*(Third Edition), Springer-Verlag, Berlin, 2008.
- [48] R.W. Floyd, Algorithm 97: Shortest path, *Commun. ACM*, 5(6) (1962) 345.

Table 1: Structures representative of protein dynamics

PDB ID code	The number of amino acids	Helical (%)	Beta sheet (%)	Exp structure
1A3H	300	38	19	X-ray
1BFG	126	8	35	X-ray
1BSN	138	26	37	NMR
2DN8	100	0	37	NMR
2DO7	101	43	9	NMR
1F39	101	3	39	X-ray
1FE6	108	90	0	X-ray
1FPR	294	30	19	X-ray
1H6T	291	17	28	X-ray
1I4S	294	68	1	X-ray
1IQQ	200	29	20	X-ray
1JLI	112	58	0	NMR
1K40	126	86	0	X-ray
1KS9	291	47	19	X-ray
1KTE	105	50	19	X-ray
1KUU	202	20	38	X-ray
1KXA	159	5	47	X-ray
1MIX	206	39	18	X-ray
1MJY	350	20	33	X-ray
1N12	298	4	55	X-ray
1OO9	294	25	17	NMR
1OOI	124	66	1	X-ray
1PHN	334	76	0	X-ray
1RAL	308	36	15	X-ray
1SUR	215	48	14	X-ray
1WUZ	103	12	34	NMR
1WWB	103	2	49	X-ray
1X0M	403	47	15	X-ray
1XGO	295	30	22	X-ray

Table 2: The exponent $h(2)$ of the time series for 29 proteins. ($Ave(h(2))$ and $Std(h(2))$ denote the average and the standard deviations of $h(2)$ for all 11 parameters of 29 proteins, respectively.)

PDB ID	Bond-p	ang-p	dih-p	imp-p	ele-p	Vdw-p	Kin-e	Tot-e	Pot-e	pre	vol
1A3H	0.6266	0.7543	0.6880	0.5951	0.9052	0.6054	0.8340	1.2845	1.0454	0.4683	0.8988
1BFG	0.6269	0.7531	0.7201	0.5790	0.9401	0.6087	0.8431	1.2971	1.0685	0.4891	0.8646
1BSN	0.6227	0.7597	0.7317	0.5792	0.9283	0.5989	0.8350	1.3072	1.0590	0.4952	0.8721
2DN8	0.6260	0.7589	0.7170	0.5848	0.9229	0.6227	0.8186	1.2910	1.0518	0.4960	0.8768
2DO7	0.6254	0.7615	0.7028	0.5823	0.9344	0.6150	0.8332	1.3074	1.0630	0.5117	0.8934
1F39	0.6334	0.7481	0.7116	0.5945	0.9267	0.6087	0.8316	1.3219	1.0593	0.5175	0.8887
1FE6	0.6265	0.7512	0.7289	0.5821	0.9383	0.6009	0.8388	1.3158	1.0662	0.5172	0.8729
1FPR	0.6262	0.7562	0.7283	0.5616	0.9021	0.5948	0.8256	1.3071	1.0423	0.4762	0.9019
1H6T	0.6263	0.7551	0.7101	0.5928	0.9300	0.6282	0.8200	1.3063	1.0715	0.5062	0.8668
1I4S	0.6270	0.7237	0.7135	0.5753	0.9367	0.6002	0.8127	1.2979	1.0688	0.4874	0.8956
1IQQ	0.6265	0.7334	0.7353	0.5893	0.9225	0.5953	0.8383	1.3070	1.0701	0.4848	0.8762
1JLI	0.6276	0.7509	0.7070	0.5673	0.9296	0.5996	0.8438	1.2918	1.0450	0.4924	0.8657
1K40	0.6253	0.7614	0.7295	0.5790	0.9278	0.6141	0.8236	1.2869	1.0648	0.5143	0.8899
1KS9	0.6232	0.7621	0.7154	0.5844	0.9184	0.5912	0.8471	1.3158	1.0575	0.4762	0.8790
1KTE	0.6267	0.7597	0.7236	0.5877	0.9230	0.5937	0.8328	1.3090	1.0584	0.4725	0.8860
1KUU	0.6262	0.7599	0.7169	0.5761	0.9125	0.6029	0.8372	1.3036	1.0638	0.4824	0.8720
1KXA	0.6263	0.7684	0.7087	0.5835	0.9251	0.6196	0.8213	1.3132	1.0466	0.5200	0.8979
1MIX	0.6401	0.7643	0.7317	0.5921	0.9418	0.6290	0.8328	1.3234	1.0571	0.5342	0.8744
1MJY	0.6269	0.7665	0.6834	0.5711	0.9290	0.5903	0.8309	1.3001	1.0481	0.5120	0.8732
1N12	0.6202	0.7530	0.7149	0.5872	0.9208	0.5965	0.8118	1.2997	1.0652	0.4719	0.9032
1OO9	0.6250	0.7639	0.7081	0.5768	0.9201	0.5907	0.8310	1.3138	1.0761	0.4779	0.8849
1OOI	0.6277	0.7565	0.7014	0.5894	0.9148	0.6012	0.8324	1.2887	1.0643	0.4757	0.8916
1PHN	0.6317	0.7603	0.7061	0.5759	0.9308	0.6022	0.8339	1.3158	1.0470	0.4898	0.8814
1RAL	0.6277	0.7580	0.7222	0.5731	0.9366	0.5940	0.8344	1.2934	1.0650	0.4822	0.8810
1SUR	0.6219	0.7569	0.7242	0.5680	0.9318	0.6038	0.8322	1.3156	1.0577	0.4903	0.8772
1WUZ	0.6340	0.7606	0.7163	0.5770	0.9274	0.6067	0.8294	1.3236	1.0575	0.5172	0.8824
1WWB	0.6555	0.7572	0.7164	0.5916	0.9274	0.6213	0.8339	1.3104	1.0717	0.5005	0.8710
1X0M	0.6205	0.7513	0.7102	0.5885	0.9172	0.6072	0.8195	1.2950	1.0460	0.4925	0.8712
1XGO	0.6103	0.7550	0.7043	0.5779	0.9335	0.6051	0.8274	1.2969	1.0691	0.4836	0.8958
Ave($h(2)$)	0.6272	0.7559	0.7147	0.5815	0.9260	0.6051	0.8306	1.3049	1.0595	0.4943	0.8823
Std($h(2)$)	0.0074	0.0090	0.0123	0.0086	0.0096	0.0110	0.0086	0.0111	0.0095	0.0174	0.0114

Table 3: The exponent λ of the horizontal visibility graphs of the time series for 29 proteins. ($Ave(\lambda)$ and $Std(\lambda)$ denote the average and the standard deviations of λ for all 11 parameters of 29 proteins, respectively.)

PDB ID	Bond-p	ang-p	dih-p	imp-p	ele-p	Vdw-p	Kin-e	Tot-e	Pot-e	pre	vol
1A3H	0.4139	0.4398	0.4236	0.4129	0.4422	0.4163	0.4282	0.6238	0.4719	0.4068	0.5088
1BFG	0.4115	0.4386	0.4274	0.4092	0.4469	0.4172	0.4293	0.6341	0.4737	0.4095	0.5032
1BSN	0.4176	0.4333	0.4276	0.4149	0.4413	0.4166	0.4270	0.6273	0.4748	0.4098	0.5086
2DN8	0.4120	0.4331	0.4264	0.4198	0.4442	0.4120	0.4309	0.6177	0.4749	0.4108	0.5038
2DO7	0.4132	0.4365	0.4301	0.4145	0.4432	0.4162	0.4240	0.6131	0.4718	0.4070	0.5068
1F39	0.4109	0.4390	0.4283	0.4113	0.4453	0.4178	0.4290	0.6243	0.4776	0.4101	0.5095
1FE6	0.4068	0.4325	0.4167	0.4177	0.4442	0.4111	0.4256	0.6239	0.4776	0.4088	0.5033
1FPR	0.4188	0.4313	0.4298	0.4158	0.4387	0.4190	0.4306	0.6229	0.4752	0.3968	0.5015
1H6T	0.4188	0.4333	0.4208	0.4121	0.4428	0.4123	0.4230	0.6239	0.4749	0.4106	0.5066
1I4S	0.4102	0.4317	0.4238	0.4145	0.4403	0.4225	0.4247	0.6299	0.4745	0.4066	0.4853
1IQQ	0.4134	0.4315	0.4245	0.4176	0.4473	0.4193	0.4238	0.6247	0.4780	0.4060	0.5046
1JLI	0.4106	0.4152	0.4224	0.4157	0.4425	0.4191	0.4286	0.6330	0.4771	0.4074	0.4772
1K40	0.4161	0.4329	0.4286	0.4158	0.4485	0.4142	0.4240	0.6213	0.4705	0.4036	0.5059
1KS9	0.4128	0.4390	0.4208	0.4188	0.4427	0.4173	0.4231	0.6296	0.4717	0.4048	0.5048
1KTE	0.4188	0.4389	0.4268	0.4141	0.4486	0.4191	0.4243	0.6292	0.4763	0.4060	0.5073
1KUU	0.4132	0.4321	0.4292	0.4143	0.4428	0.4183	0.4266	0.6264	0.4792	0.4030	0.5035
1KXA	0.4111	0.4254	0.4285	0.4197	0.4352	0.4126	0.4240	0.6397	0.4733	0.4032	0.5033
1MIX	0.4163	0.4332	0.4266	0.4199	0.4490	0.4193	0.4265	0.6381	0.4794	0.4086	0.5041
1MJY	0.4176	0.4326	0.4254	0.4142	0.4430	0.4197	0.4231	0.6128	0.4793	0.4079	0.5028
1N12	0.4174	0.4236	0.4206	0.4180	0.4477	0.4197	0.4260	0.6276	0.4729	0.4022	0.5081
1OO9	0.4182	0.4371	0.4210	0.4094	0.4422	0.4170	0.4220	0.6297	0.4704	0.4058	0.5067
1OOI	0.4144	0.4315	0.4212	0.4161	0.4408	0.4162	0.4266	0.6212	0.4753	0.4085	0.5027
1PHN	0.4133	0.4255	0.4229	0.4132	0.4422	0.4186	0.4250	0.6328	0.4719	0.3952	0.5037
1RAL	0.4173	0.4303	0.4255	0.4166	0.4437	0.4103	0.4221	0.6308	0.4744	0.4003	0.4936
1SUR	0.4145	0.4350	0.4278	0.4164	0.4445	0.4189	0.4259	0.6439	0.4787	0.4076	0.4905
1WUZ	0.4152	0.4300	0.4265	0.4189	0.4423	0.4158	0.4217	0.6046	0.4747	0.4076	0.5063
1WWB	0.4103	0.4361	0.4231	0.4151	0.4460	0.4174	0.4237	0.6269	0.4799	0.4089	0.5065
1X0M	0.4155	0.4339	0.4246	0.4102	0.4426	0.4181	0.4268	0.6210	0.4778	0.4089	0.4953
1XGO	0.4169	0.4309	0.4215	0.4144	0.4447	0.4141	0.4227	0.6282	0.4712	0.4094	0.5020
Ave(λ)	0.4144	0.4325	0.4249	0.4152	0.4436	0.4168	0.4255	0.6263	0.4751	0.4063	0.5023
Std(λ)	0.0031	0.0052	0.0033	0.0029	0.0030	0.0029	0.0026	0.0081	0.0029	0.0038	0.0073

Table 4: The fractal dimension d_B of the horizontal visibility graph of the time series for 29 proteins. (Ave(d_B) and Std(d_B) denote the average and the standard deviations of d_B for all 11 parameters of 29 proteins, respectively.)

PDB ID	Bond-p	ang-p	dih-p	imp-p	ele-p	Vdw-p	Kin-e	Tot-e	Pot-e	pre	vol
1A3H	2.2420	1.9094	2.0924	2.1066	1.6176	2.2444	1.8359	1.1711	1.4636	2.3378	1.7238
1BFG	2.1676	1.9819	2.0500	2.2011	1.6010	2.2705	1.8846	1.1743	1.4867	2.2933	1.6836
1BSN	2.2406	1.9308	2.0763	2.1631	1.6173	2.2659	1.8608	1.1663	1.4840	2.3774	1.6850
2DN8	2.1980	1.9635	2.1620	2.1677	1.6223	2.2684	1.8451	1.1764	1.4928	2.3181	1.8107
2DO7	2.1975	1.9583	2.0344	2.1446	1.6304	2.3466	1.8794	1.1816	1.5028	2.3746	1.7386
1F39	2.2468	1.9891	2.1464	2.1154	1.5909	2.2725	1.8349	1.1857	1.4706	2.2654	1.6819
1FE6	2.2630	2.0082	2.0136	2.1567	1.6369	2.3287	1.8510	1.1717	1.4698	2.2609	1.7250
1FPR	2.2390	1.9955	2.1629	2.2214	1.6071	2.3019	1.8316	1.1665	1.4861	2.3601	1.7634
1H6T	2.3016	1.9043	2.0813	2.1474	1.6370	2.2001	1.8580	1.1864	1.4765	2.3218	1.7400
1I4S	2.2240	2.0261	2.0840	2.0849	1.6208	2.2055	1.8901	1.1820	1.5158	2.3245	1.7718
1IQQ	2.2468	1.9935	2.0428	2.2282	1.6163	2.2704	1.8316	1.1674	1.4841	2.4346	1.7014
1JLI	2.2892	2.0062	2.0662	2.1833	1.6201	2.3098	1.8878	1.1816	1.4788	2.2764	1.7530
1K40	2.1872	1.9844	2.0558	2.1804	1.6435	2.2935	1.8767	1.1773	1.4626	2.4219	1.7508
1KS9	2.2384	1.9884	2.0947	2.0910	1.6336	2.3056	1.8368	1.1753	1.4988	2.3386	1.7253
1KTE	2.1812	2.0072	2.0802	2.0754	1.6411	2.2450	1.8494	1.1789	1.4744	2.3078	1.7542
1KUU	2.1128	2.0287	2.1360	2.1860	1.6510	2.2234	1.8746	1.1909	1.4877	2.3736	1.7157
1KXA	2.1854	1.9436	2.0970	2.1582	1.6303	2.3596	1.8813	1.1700	1.5108	2.2604	1.7123
1MIX	2.2149	2.0408	2.1175	2.1299	1.6383	2.3023	1.8498	1.1522	1.4852	2.3154	1.7070
1MJY	2.1973	1.9703	2.0800	2.1877	1.6672	2.2188	1.9019	1.1565	1.4943	2.3145	1.7069
1N12	2.2549	2.0646	2.0082	2.0736	1.6065	2.2561	1.8471	1.1778	1.4863	2.3750	1.7865
1OO9	2.2266	2.0059	2.0746	2.0948	1.6369	2.3035	1.8906	1.1750	1.4822	2.3019	1.7576
1OOI	2.2811	1.9514	2.1226	2.1475	1.6275	2.2415	1.8729	1.1746	1.4662	2.2810	1.7851
1PHN	2.2882	1.9190	2.0631	2.1411	1.6152	2.3023	1.8914	1.1673	1.4838	2.4080	1.7280
1RAL	2.1851	2.0142	2.0490	2.0774	1.6226	2.2371	1.8833	1.1743	1.4981	2.3651	1.7658
1SUR	2.2318	2.0036	2.0301	2.0664	1.6251	2.2950	1.9093	1.1901	1.4917	2.2883	1.7264
1WUZ	2.2801	1.9021	2.0407	2.1896	1.6406	2.3845	1.8850	1.1693	1.5043	2.4449	1.6824
1WWB	2.2323	1.9986	2.0172	2.1306	1.6187	2.3751	1.8956	1.1743	1.4875	2.2518	1.7267
1X0M	2.2126	2.0268	2.0530	2.1421	1.6553	2.2801	1.8780	1.1676	1.4813	2.3462	1.7104
1XGO	2.1929	2.0190	2.0762	2.1694	1.6323	2.3051	1.8543	1.1876	1.4716	2.3140	1.7302
Ave(d_B)	2.2262	1.9840	2.0761	2.1435	1.6277	2.2832	1.8695	1.1748	1.4855	2.3328	1.7327
Std(d_B)	0.0424	0.0422	0.0419	0.0456	0.0164	0.0474	0.0233	0.0090	0.0134	0.0533	0.0331

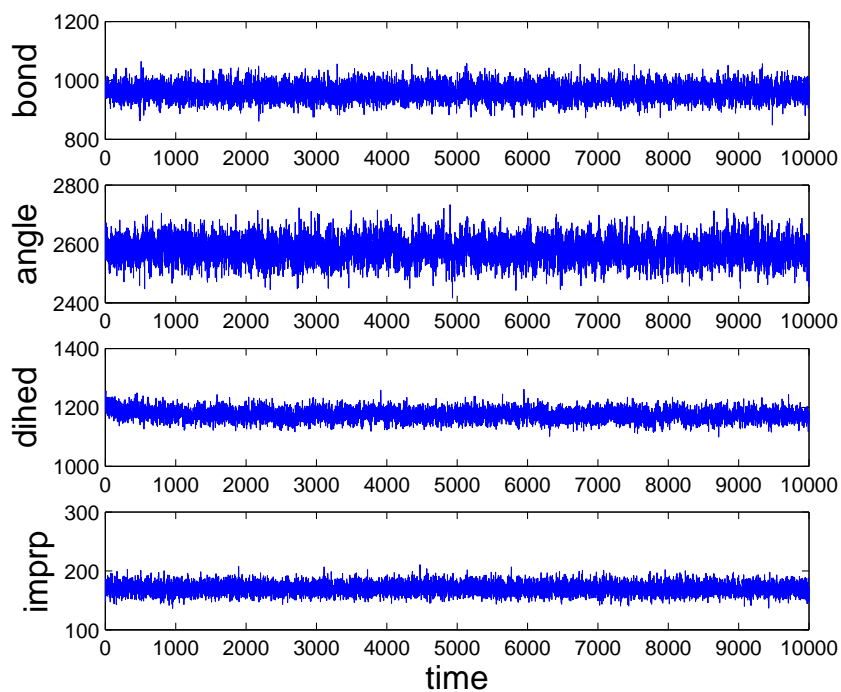


Figure 1: Bonded potential, angle potential, dihedral potential and improper potential time series for protein 1A3H.

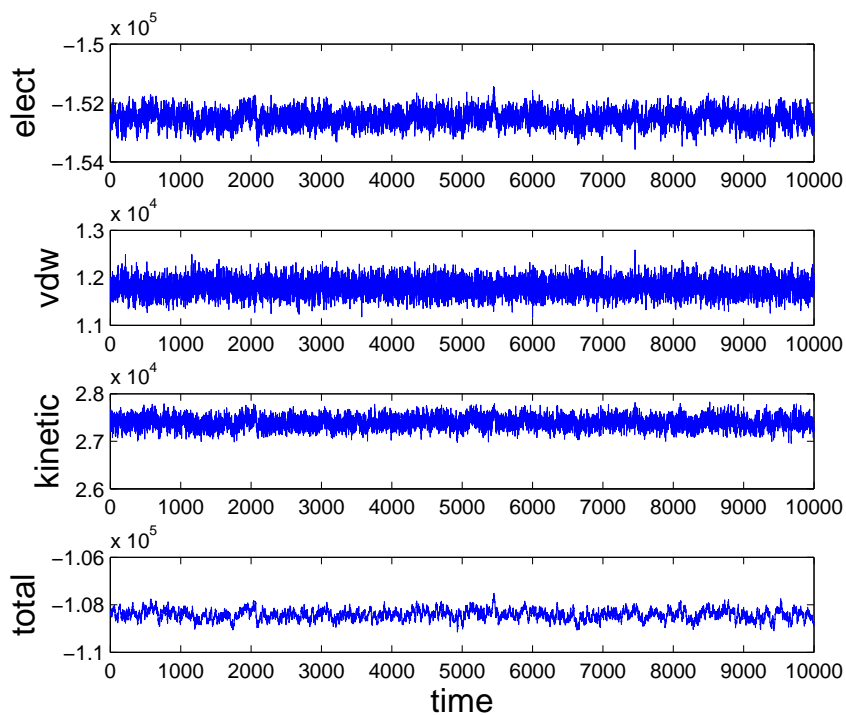


Figure 2: Electrostatic potential, Van der Waals potential, kinetic energy and total energy time series for protein 1A3H.

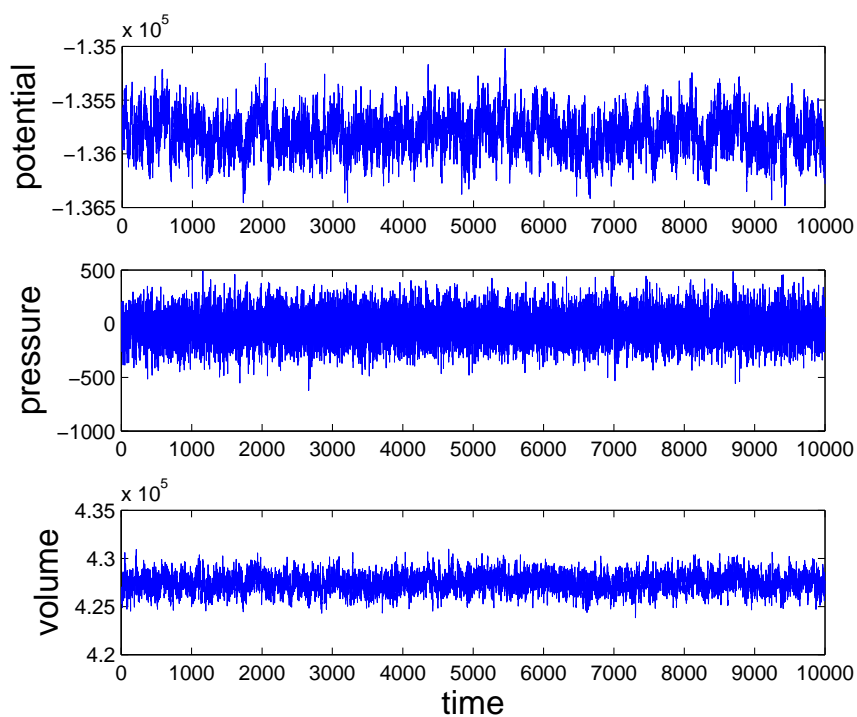


Figure 3: Potential energy, pressure, and volume time series for protein 1A3H.

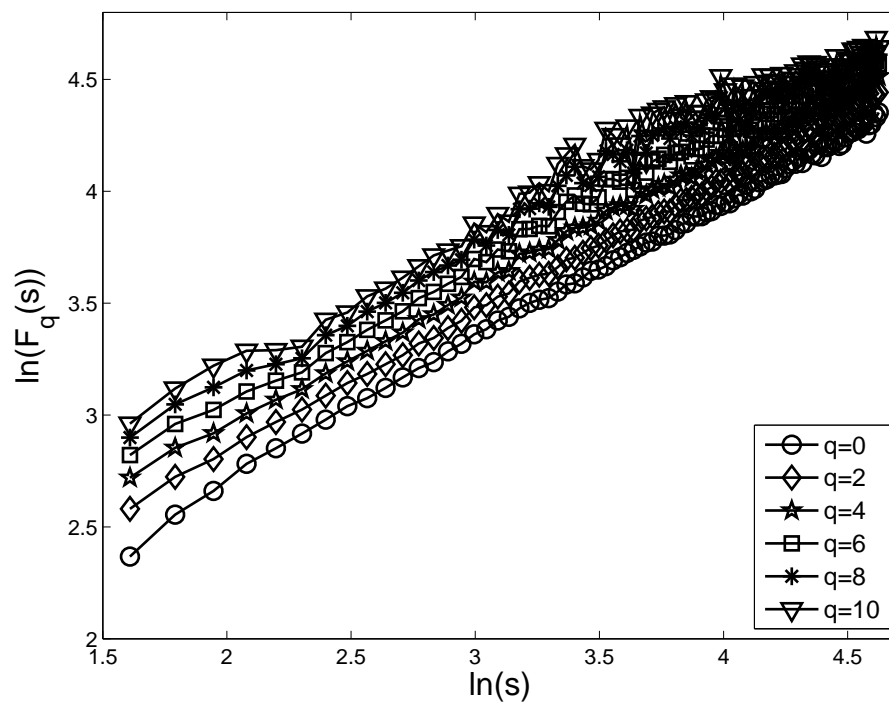


Figure 4: Linear regressions for calculating the exponents $h(q)$ for the bonded potential time series of protein 1A3H.

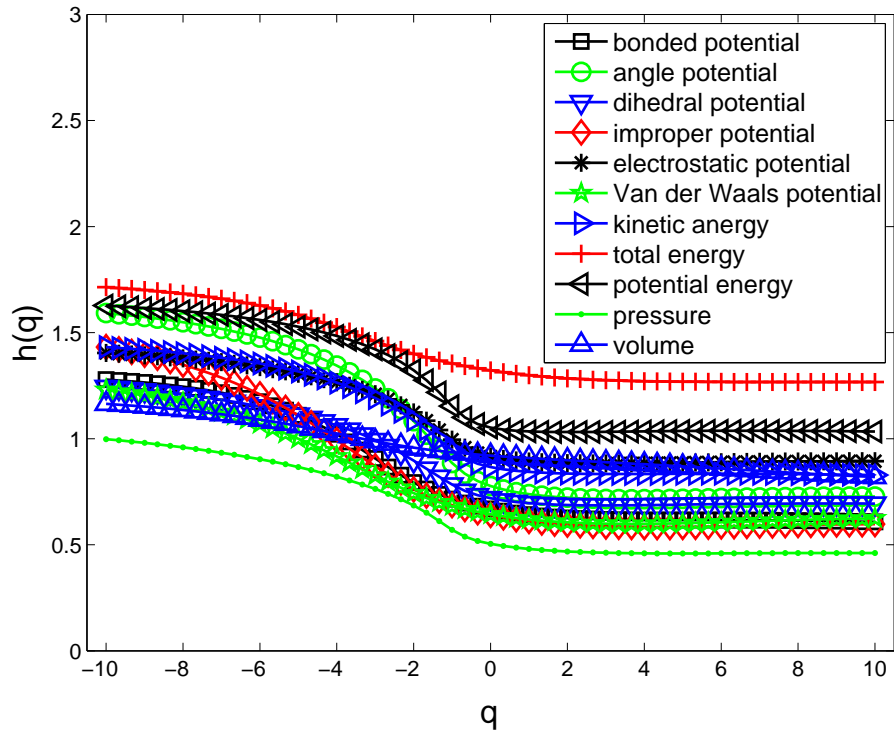


Figure 5: Multifractal $h(q)$ curves for the energy, pressure and volume time series of protein 1A3H.

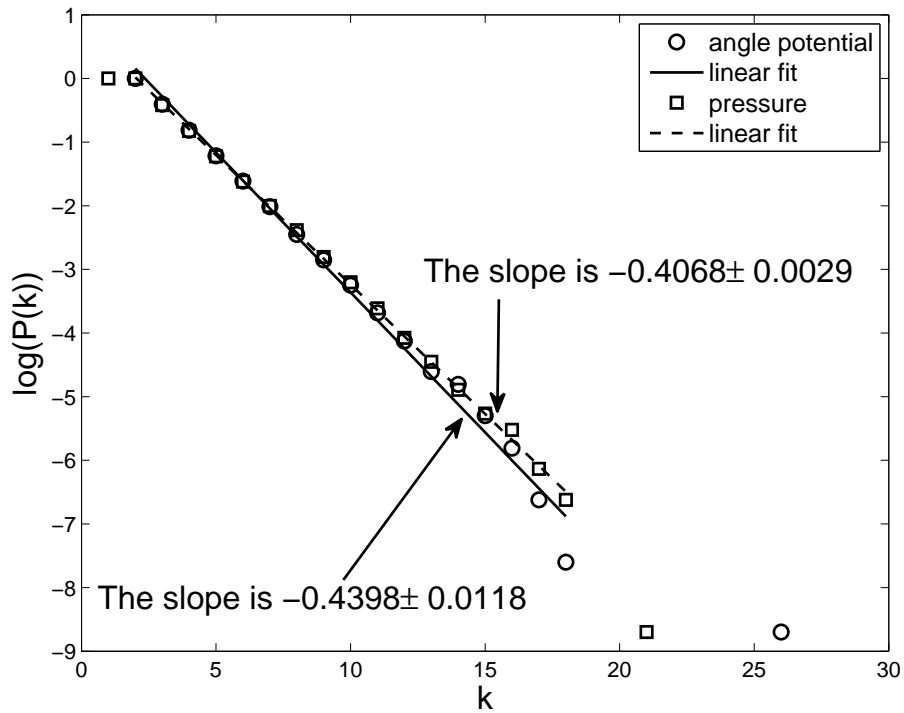


Figure 6: The degree distributions $P(k)$ of the horizontal visibility graph for the angle potential and pressure time series of protein 1A3H.

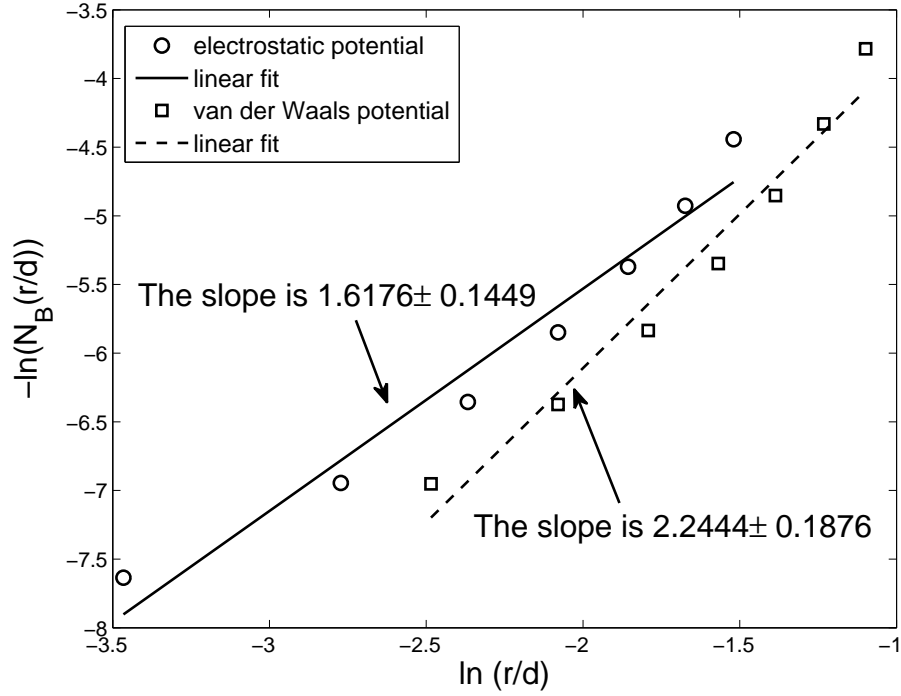


Figure 7: Linear regressions for calculating the fractal dimensions d_B of the horizontal visibility graphs for the electrostatic potential and van der Waals potential time series of protein 1A3H.

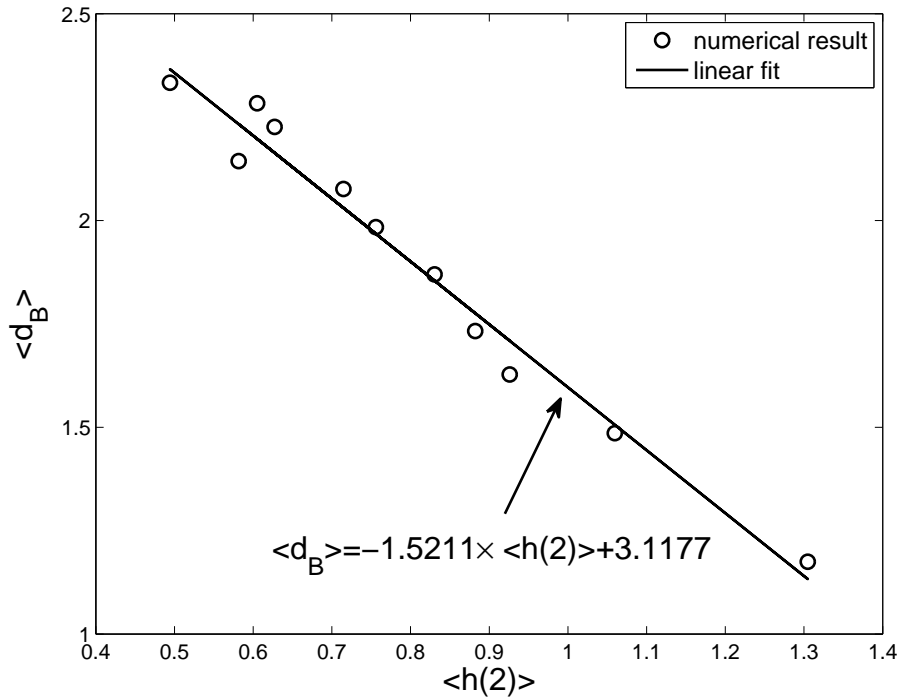


Figure 8: The relationship between $\langle h(2) \rangle$ (from MF-DFA on time series) and $\langle d_B \rangle$ of the constructed horizontal visibility graphs for different energy, pressure and volume. The average is taken over 29 proteins.